Manchester Metropolitan University

e-space

Manchester Metropolitan University's Research Repository

Please cite the Published Version

Greenwood, Thomas and Koehler, Sven PK (2021) Nitric Oxide Scattering off Graphene Using Surface-Velocity Map Imaging. The Journal of Physical Chemistry C, 125 (32). pp. 17853-17860. ISSN 1932-7447

DOI: https://doi.org/10.1021/acs.jpcc.1c05014

Publisher: American Chemical Society

Version: Accepted Version

Downloaded from: https://e-space.mmu.ac.uk/628232/

Usage rights: © In Copyright

Enquiries:
If you have questions about this document, contact openresearch@mmu.ac.uk. Please include the URL of the record in e-space. If you believe that your, or a third party's rights have been compromised through this document please see our Take Down policy (available from https://www.mmu.ac.uk/library/using-the-library/policies-and-guidelines)

Nitric Oxide Scattering off Graphene using Surface-Velocity Map Imaging

Thomas Greenwood, *Sven P. K. Koehler*[*]

Department of Natural Sciences, Manchester Metropolitan University, M1 5GD, UK

*Corresponding author.

Email: s.koehler@mmu.ac.uk

Manchester Metropolitan University

Department of Natural Sciences

Manchester

M1 5GD

United Kingdom

Abstract

We investigated the scattering of nitric oxide, NO, off graphene supported on gold. This is of fundamental importance to chemistry as collisions are the necessary first step to chemical reactions on graphene, and nitric oxide molecules are inherently radicals, with the potential to bond to graphene. We directed a molecular beam of NO in helium onto graphene and detected the directly scattered molecules using surface-velocity map imaging. In contrast to previous scattering studies off graphite which detected only a modest reduction of the translational energy of the NO, we observe a loss of ~80% of the molecules' kinetic energy. Our classical molecular dynamics simulations still predict a loss of ~60% of the translational energy in the scattering process. This energy appears to partly go into the NO rotations, but mostly into collective motion of the carbon atoms in the graphene sheet. At 0° incidence angle, we also observe a very narrow angular scattering distribution. Both findings may be unique to pristine graphene on gold as 1) the 2D honeycomb structure is perfectly flat, and 2) the graphene is only loosely held to the gold at a distance of 3.4 Å, thus it can absorb much of the projectiles' kinetic energy.

Keywords: graphene, scattering, velocity map imaging, surface scattering, REMPI, nitric oxide

TOC Graphic:

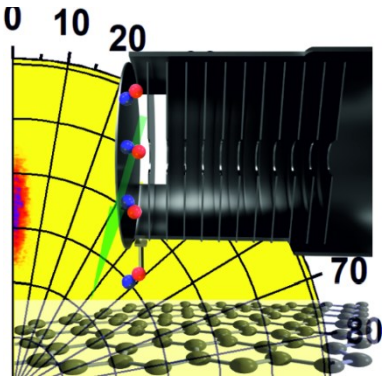

1. Introduction

Chemical reactions are at the very heart of chemistry,[1] and collisions between reactants are a necessary first steps towards any chemical reaction.[2] Collisions between gas-phase species, both non-reactive and reactive processes, have hence long been studied in the field of reaction dynamics in order to understand the re-distribution of energy.[3] Equally, the investigation of the detailed scattering dynamics of gas-phase species off surfaces has a long tradition,[4] not least because of its enormous importance for heterogeneous catalysis.[5] Reactive and non-reactive scattering,[6,7] adsorption and (photo-)desorption[8] studies have all been performed on various types of solid surfaces incl. metal single crystals, metal oxides, and stepped and corrugated surfaces, to name a few. Graphite surfaces have also heavily featured in surface scattering experiments,[9] and more recently graphene, a 2-dimensional hexagonal arrangement of sp^2-hybridized C-atoms.[10]

Graphene research has increased exponentially since the discovery of its remarkable electronic, physical, and chemical properties almost 20 years ago.[11] Some of these properties such as the band gap (pristine graphene is a zero band gap material) can be tuned by functionalization through chemical reactions on graphene, and we have in our group modified CVD graphene with functional groups such a phenyl groups or hydrogen atoms, and investigated these graphene derivatives using sum-frequency generation spectroscopy.[12,13]

Studies of the detailed scattering dynamics of actual collisions on graphene that potentially lead to the formation of such functionalised graphene derivatives have recently emerged. It is important in this context to remember that graphene is a surface held together by a 2D network of covalent bonds, and collisions between (reactive) species and graphene could potentially lead to truly covalent bond formation.

Minton and co-workers measured the kinetic energy and angular distribution of N_2 scattered off highly oriented pyrolytic graphite (HOPG) in sophisticated molecular beam experiments coupled with classical molecular dynamics (MD) simulations. They found that the N_2 1) scatters off after a single collision, or is 2) temporarily or 3) permanently trapped at the surface.[14] Hase and co-workers modelled the collisional dynamics of N_2 with graphite at collision energies of 26 kJ mol^{-1} and 60 kJ mol^{-1} and found that for all incidence angles, single collision scattering is the dominant process; at the lower collision energy (similar to what is used in our work here) close to normal incidence angles, roughly 50% of the initial translational energy is channelled away, primarily to the graphene surface vibrational modes.[15] This was taken one step further by Nieman *et al.* and Jayee *et al.* in their primarily modelling studies of the reaction of N(^{4}S) and O(^{3}P) atoms with graphene, though at vastly higher collision energies relevant to the re-entry of spacecrafts into Earth's atmosphere.[16,17] Both the high collision energy as well as the fact that a reactive atomic species is scattered off graphene cause not only non-reactive scattering to be observed, but also reactions with the graphene itself (functionalisation), and the formation of ablation products such as CN radicals in the gas-phase. Juaristi and co-workers modelled the scattering of O_2 off HPOG by *ab initio* molecular dynamics at lower collision energies of ~20 kJ mol^{-1}, focusing on the effects of the initial alignment of the impinging O_2 molecule.[18]

Many early state-resolved studies were concerned with the collision dynamics of NO with graphite.[19] It seems as if specular scattering dominates at higher temperatures, whereas an isotropic scattering due to trapping desorption is dominant at lower temperatures.[20] However, later studies by Walther and co-workers found no diffusely scattered molecules at surface temperatures below 70 K, with only the inelastic scattering channel remaining.[21] When angular distributions were investigated – typically at incidence angles varying from 45° to 60° – the direct channel displayed

a narrow distribution but still with a width of 10° or more.[22] Even at fairly steep incidence angles of 30°, Frenkel *et al.* still observed a diffuse isotropic trapping component, and a width of the angular distribution of the specular component of ~20°.[23]

As far as reactions on graphene go, hydrogenation is probably the simplest modification to graphene,[13,24] and the reactivity has been modelled by Lischka and co-workers,[25] and also investigated both in rather elegant dynamics experiments as well as modelled by Wodtke and co-workers.[26,27] A short pulse of H atoms was scattered off graphene under UHV conditions, and the angular and kinetic energy distribution extracted by detecting the hydrogen using an H-atom Rydberg tagging scheme. Most strikingly, evidence for temporary bond formation between the H atoms and graphene was found.

Velocity Map Imaging (VMI) is one of the most successful recent techniques to probe reaction dynamics;[28,29] VMI is typically applied to gas-phase dynamics, but more recently expanded to surface processes,[30,31,32,33,34] and we have ourselves applied it to the laser-desorption of NO from gold single crystals.[35,36] Surface-VMI not only delivers the velocity (i.e. speed and angular) distribution of scattering products after surface collision, but due to the REMPI scheme frequently employed, can also establish the vibrational and rotational state distribution of the scattered products. We hence chose to perform surface-VMI collision experiments by scattering nitric oxide off graphene, because 1) NO is intrinsically a radical and can hence potentially react with the graphene substrate, and 2) because NO as a diatomic molecule allows us to also investigate the internal energy distribution after scattering off graphene.

2. Experimental Methods

Our surface-VMI apparatus has been described previously,[37,38] but a number of key features and changes warrant a more detailed description. The spectrometer consists of two vacuum chambers,

the first housing the molecular beam (firing vertically downwards in the lab frame), and the second chamber houses the graphene surface on a gold substrate, together with the twelve VMI optics plates and the multi-channel plate detector/phosphor screen assembly. The chambers are each evacuated using 1000 L s^{-1} turbomolecular pumps which in turn are backed by their own rotary pumps to achieve a base pressure in the main chamber below 5×10^{-9} Torr. The molecular beam consists of a 2-4% NO mixture seeded in He which is supersonically expanded through a pulsed valve (500 μm diameter orifice, 300 μs opening time) to a velocity of ~1500 m s^{-1}. The NO molecules travel ~27 cm downwards into the space between the first two VMI plates where they are intersected by the laser beam, crossing horizontally through the center of the chamber between those first two plates. The NO molecules travel a further ~5 cm and scatter off the graphene surface, recoiling to cross the laser beam a second time in the center of the VMI optics. The three axes of 1) probe laser along *x*, 2) counter-propagating molecular beam (from top)/surface normal (with the surface near the bottom of the VMI optics in the lab frame), *y*, and 3) the time-of-flight (TOF) axis of the VMI apparatus, *z*, are mutually perpendicular as shown in Figure 1 a). We have chosen this *xyz* axes labelling as the *x* and *y* axis in the lab frame are now the same as the *x* and *y* dimension of the resulting 2D VM images. We highlight that this positioning of the surface within the VMI optics is a departure from our previous work in which the surface normal was aligned along the main axis of the TOF spectrometer, and which delivered velocity distribution in all three dimensions in space independently. However, due to the much longer timescales of a molecular beam pulse compared to a laser pulse, we are losing this timing option in the current scattering experiments, and hence have to extract the speed along the surface normal from the *y* coordinate of the VM images instead. The remaining *x* dimension of the images delivers – after appropriate transformation – the polar angle distribution. For scattering experiments from a flat surface as

described here, it is reasonable to assume a homogeneous azimuthal distribution around the surface normal, and hence only the velocity component along the surface normal and one velocity component parallel to the surface need to be measured.

The grounded surface is positioned ~5 cm below the laser beam axis close to a grounded shield surrounding the ion optics, and as such does not disturb the VMI field in the ionization region noticeably, see Figure 1 b). Previous research on the scattering off liquid surfaces by Greaves and co-workers employing a similar geometry to image the scattering plane used an elegant arrangement involving charged razor blades in order to ensure that the field lines between the ion plates are not distorted.[33] We note, however, that the distance between the ionization region and the surface in those experiments is much shorter (i.e. the surface is placed *in-between* the first two ion plates), but thanks to the ease with which NO can be laser-ionized here, we can afford to locate the surface much further away from the laser beam and in fact close to the ground shield surrounding the ion optics, such that the field lines in the central region of the VMI spectrometer are not distorted. Wodtke and co-workers use a shorter flight distance in a similar setup and crucially a fs laser to non-resonantly ionize desorbed molecules, and can conveniently switch between spatial and velocity map imaging,[34] while on the other hand the ease of (1+1) REMPI detection in our setup negates the need for a focussing lens, and we do not need to scan the probe laser across the ionization region. The longer flight path from the surface to the ionization laser potentially limits the width of the angular distribution that can be recorded, but since the detection laser is not focused (and hence all ionized NO molecules with a clear trajectory to the detector are recorded, up to 12.5 mm either side of the centre of the VMI optics), we appear to record a much narrower polar angle distribution of the scattered NO molecules than theoretically possible, i.e. we are *not* biasing against NO molecules at larger polar angles. We note that the exact distance

between the surface and the laser is not required as we extract the velocity from the VM images, and *not* from time-of-flight times to the laser.

The surface is resting (i.e. no spring clips used that would cover part of the surface) on a surface holder mounted on a manipulator, and the sample itself consists of a silicon wafer onto which a thin layer of chromium and then gold has been evaporated, covering the whole wafer, before graphene – CVD-grown on copper – was transferred onto the gold. The correct vertical alignment of the surface normal was checked by shining a He:Ne laser pointer along the central *y* axis of the chamber (in-line with the molecular beam), and ensuring that the back-reflection from the wafer travels along the same path as the incoming beam, guaranteeing that the surface normal is aligned with the molecular beam.

Nitric oxide molecules are ionized ~5 cm above the surface using a (1+1) REMPI scheme via the A ← X transition. The third harmonic of a Continuum Surelite II-10 Nd:YAG laser was used to pump a Radiant Dyes NarrowScan laser using Coumarin 450 dye, and the dye laser output was then frequency-doubled using a BBO crystal to achieve ~226 nm laser pulses at 10 Hz with a pulse energy of ~0.8 mJ.

The ionized NO particles are then accelerated over a potential difference of 1000 V towards a multi-channel plate (MCP) detector coupled to a phosphor screen. The MCP is pulsed at 10 Hz to reduce background noise caused by ions other than NO^+. We do not 'DC-slice' the ion cloud as the long flight path from the scattering region to the ionization region causes our images to be optically sliced, essentially imaging one scattering plane (the *x*-*y* plane). The phosphor screen captures the ions' positions and image acquisition is performed by a 10 Hz synchronized camera (NET C-IC4133BU-U3V) connected to a personal computer via a National Instruments PCIe-8242 frame grabber.

Since we are not operating a molecular beam directed along the spectrometer's time-of-flight axis, we have to establish the central spot (equating to zero velocity along the *x* and *y* dimension and hence essential for image analysis) on the detector by different means: instead we back-fill the chamber with pure nitric oxide at a background pressure of 2×10^{-7} Torr;[39] ionizing this thermal gas ensemble yields a 2-dimensional Maxwell-Boltzmann distribution on the detector with a peak along *x* and *y* at 0 m s^{-1} each, thus establishing the center of our images. Calibration of the VMI setup was performed by NO_2 dissociation at ~226 nm as previously described.[38,40]

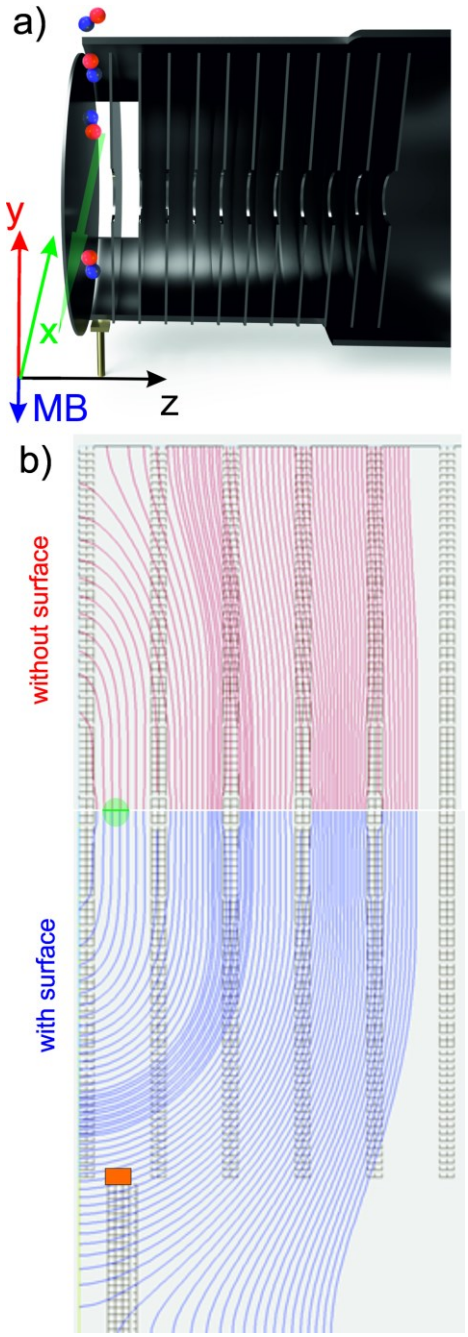

Figure 1: a) Cutaway CAD drawing of our 12-plate ion optics with the molecular beam indicated; faint green arrow is the REMPI laser beam between the two plates furthest left; *x*- (along laser beam) and *y*-dimension (parallel to the molecular beam and surface normal; surface shown in gold near the bottom) chosen as these are the dimensions which yield the velocity maps' *x*-*y* coordinates; *z* is along the time-of-flight direction. b) SIMION simulations of the electric fields without (red) and with (blue) the surface in place. Grounding shield omitted for

3. Computational Methods

All molecular dynamics simulations here were performed within the DL_POLY Classic suite using a combination of force fields.[41] A simulations box was selected with a parallelogram as a base (in the *x*-*y* plane) and periodic boundary conditions along the two dimensions of that base (parallel to the interfaces present here), but with no periodicity in the *z* direction which is along the surface normal. The substrate was formed of a 6×6×6 array of gold atoms whose interactions were described by a Gupta potential.[42] 98 carbon atoms were positioned in a hexagonal 2D network in the *x*-*y* plane on top of the gold substrate. The bonds in the graphene sheet were described by a harmonic potential (rather than fixed bond lengths) to accurately reflect any compressions and stretches in the bonds as the NO collides with the graphene surface. A Morse bond potential described the C-C bonds with parameters proposed by Kalosakas *et al.*,[43] using the accepted carbon-carbon internuclear distance in graphene of 1.42 Å, with $D = 5.7$ eV and $\alpha = 1.96$ Å^{-1}. Angles and dihedrals were described by quartic and cosine functions, respectively.[43] This system was relaxed by running simulations in an *NVT* ensemble regulated to 300 K by a Nosé-Hoover thermostat for 4 ns with a relaxation constant of 1 ps. A single nitric oxide molecule was then placed in a randomly selected position in the *x*-*y* plane, but ~18 Å above the graphene surface. The nitric oxide bond was described by a Morse potential with parameters $D_e = 6.61736$ eV, $\alpha = 2.636$ Å^{-1} and $r_e = 1.151$ Å.[44] To complete the force field, non-bonding interaction were described by Lennard-Jones 12-6 potentials, with parameters either provided by the force fields above, or taken from the universal force field set out by W. M. Skiff and co-workers,[45] with the exception of the gold and graphene interaction being developed by E. E. Helgee and A. Isacsson.[46] Lorentz-Berthelot combining rules were applied for interactions between unlike atoms. Interatomic forces were truncated after 7 Å. It should be noted that more

sophisticated neural network potential energy surfaces have recently been calculated even for surface scattering processes related to the one presented here,[47,48,49] however, not all of these studies take the metal substrate into account, and the literature force fields mentioned above – while not verified for the NO-graphene interaction – are likely to be sufficient to at least qualitatively reproduce the trends observed experimentally.

The NO was directed at the graphene either N- or O-head first with 1600 m s^{-1} along the surface normal, and 2000 trajectories were run and analyzed for each orientation. After collision with the graphene, the NO was detected once traversing a virtual plane 8 Å above the graphene, where there is no longer any interaction between the graphene and the NO. Properties such as the velocity components of both the N and O atoms in all three dimensions separately were recorded. Molecular speeds and polar angles were calculated from center-of-mass shifts and binned in 20 m s^{-1} and 5° wide intervals, respectively.

4. Results and Discussion

Figure 2 a) shows an overlay of three ion images all of which were recorded on the $Q_1(0)$ line of the A ← X transition of NO as per Figure 2 b), but control experiments on the $R_1(0)$ line yield the same results. The signal due to the molecular beam travelling towards the surface is shown in blue, while the scattered signal is shown in red. The scattered signal was recorded at a time delay (between the molecular beam and the probe laser) which was increased by 100 μs compared to the molecular beam images; this is to account for the round-trip time from the laser to the surface and back (~10 cm) such that we probe 'the same' directly scattered NO molecules whose velocity distribution in the molecular beam we established before collision with the graphene. Finally, the more diffuse spot in the middle in green is from the ionization of thermal background NO (p_{bg} = 5 × 10^{-7} Torr), and this image is fitted to a 2-dimensional Maxwell-

Boltzmann velocity distribution. In absence of a molecular beam aligned along the main VMI axis, the center spot of this distribution, highlighted in the image as a green cross, corresponds to our zero velocity coordinate.

The speed distributions shown in Figure 3 a) are established relative to this zero velocity coordinate (which does not vary by more than one pixel or 5.1 m s^{-1} from day to day) and after application of the appropriate density-to-flux conversion by multiplication with the speed.[50] The initial molecular beam (blue) and the scattered molecules (red) are naturally in opposite directions. All distributions are fitted to equation 1 as we are measuring a 2D distribution

$$F(c)\mathrm{d}c = A\, c^2 \exp \frac{-(c - c_0)^2}{\alpha^2}\, \mathrm{d}c \qquad \text{eqn. 1}$$

where A is a scaling factor and α is related to the width of the distribution.[51] While the NO in the molecular beam has an average kinetic energy $\langle E_{kin} \rangle$ of 0.31 eV (30 kJ mol^{-1}), the scattered NO has lost around 80% of its kinetic energy, down to 0.06 eV; this is a much greater loss of kinetic energy than observed in the direct channel of the NO scattering off graph**ite**.[23] In the simplest form of the Baule model and assuming collision with one surface C atom only, the NO would not scatter off the surface at all due to the much larger mass of NO compared to a single C atom in graphene.[52,53] Instead, the Baule model predicts that the mass equivalent of just over six C atoms together would account for the observed energy loss of the projectile, which is not unrealistic given the tight covalent network of the 2D lattice, though the fact that the number of C atoms is close to one hexagon in graphene is likely coincidental. The translational energy distribution is – as expected – also broader than the initial molecular beam. Despite this dramatic energy loss, the scattered NO cannot be described as thermal. We have attempted to fit the scattered data to the equation describing a Maxwell-Boltzmann distribution for desorption from a surface,[54] but obtained a worse fit which did not reproduce the experimental data as well. This indicates that

the dominant scattering channel in our case of 0° incidence angle is a direct scattering mechanism, but associated with a significant loss of energy which most likely goes into the collective motion of the carbon atoms in graphene. Efficient transfer of energy to the substrate's phonon modes has also been observed e.g. for NO scattering of Ag(111).[55] We observe a diffuse and very weak spot at slower NO velocities that could be due to a trapping-desorption

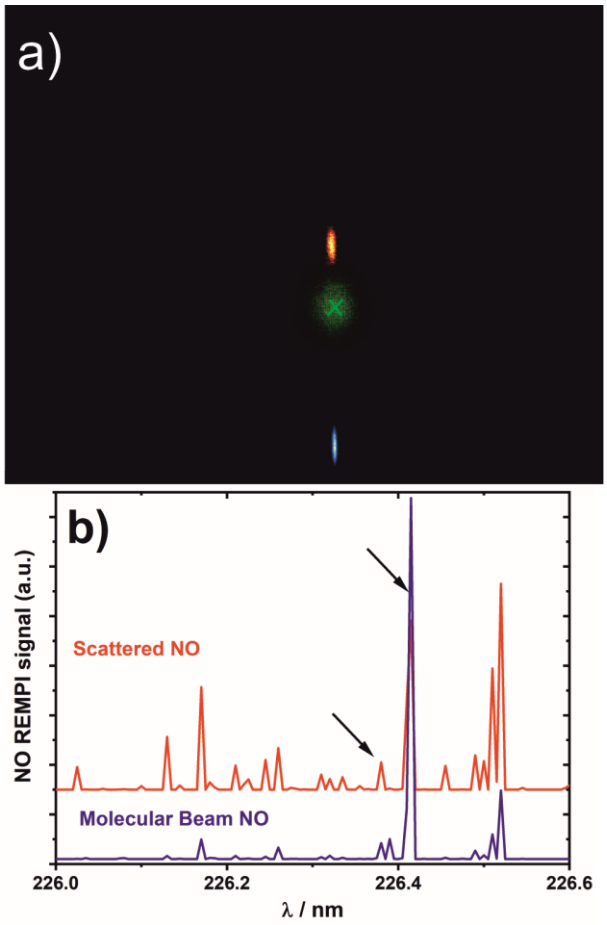

Figure 2: a) Overlay of three velocity map images of nitric oxide, NO. The downward facing molecular beam is in blue, the scattered NO in red, and the diffuse green spot in the center is thermal background NO gas, imaged to define the zero velocity coordinate (illustrated by the green cross). b) Rotationally-resolved REMPI spectra of NO in the molecular beam (blue), and scattered off graphene (red). Black arrows point to the $Q_1(0)$ and $R_1(0)$ lines on which most images were recorded.

mechanism, but this channel is far less pronounced compared to the directly scattered NO. While the spectra shown in Figure 2 b) demonstrate that some energy is channelled into rotational degrees of freedom, this only accounts for a small fraction of the lost energy. Much of the earlier work on collisions of NO with graphite had focused on the rotational distribution of the inelastically scattered NO,[56,57] and found evidence for *rotational cooling.* For the vibrationally elastic scattering of NO(v=3) off Au(111), NO loses around half its initial kinetic energy for incidence energies close to those employed here; interestingly, the final kinetic energy of the NO decreases with increasing rotational state,[58] an effect we have not been able to probe yet. While a complete analysis of the rotational state population is reserved for a later publication, with the focus here on the velocity distributions, we have not been successful in detecting NO(v = 1) in the scattered beam; this is in contrast to e.g. nitric oxide scattering off metal single crystal surfaces such as Au(111) at similar incidence energies,[59] during which fractions of a percent of NO(v = 1) were detected at surface temperatures close to the room temperature graphene employed here.

The results of our classical molecular dynamics simulations in which NO molecules were approaching the graphene surface with a velocity of 1600 m s^{-1} along the surface normal (black vertical arrow in Figure 3 a) and collided with the graphene in a random position were fitted to the 3D variant of equation 1 (replacing the c^2 with a c^3), see black data in Figure 3 a). There is

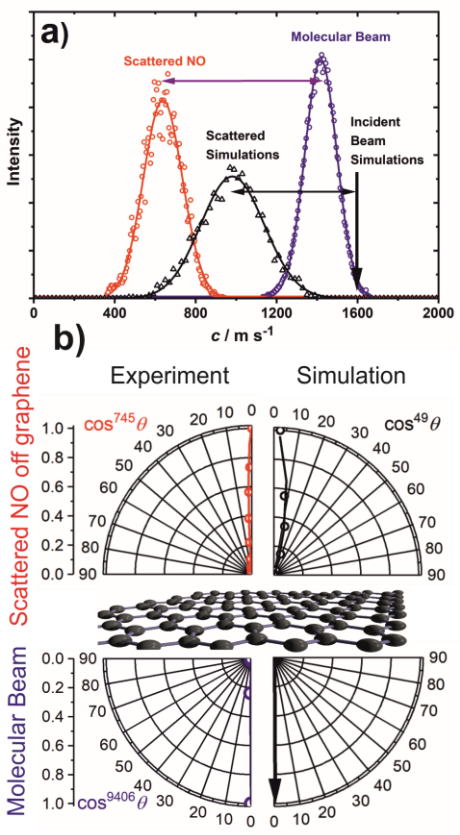

Figure 3: a) Speed distributions extracted from the VM images in Figure 2 for the molecular beam in blue, and the scattered NO in red; the black data are results of molecular dynamics simulations commencing with monoenergetic NO molecules at 1600 m s^{-1}, indicated by the black arrow; all data (open symbols) fitted to equation 1 (lines). b) Polar angle distribution of: bottom panels for the molecular beam, and top panels for the scattered NO; left panels are experimental data, right panels molecular dynamics simulations. Open circles are data points, lines are fits to a $\cos^n\theta$ function as shown.

some qualitative agreement in that the scattered NO molecules lose more than 60% of their mean kinetic energy (from 0.4 to 0.15 eV), but this energy loss is less pronounced compared to the experiments. This discrepancy is likely due to the limitations of the employed force field and could be improved using DFT-based force fields,[47,48,49] but the overall trend observed is reproduced qualitatively. Future scattering experiments with aligned NO molecular beams could serve as a benchmark for improving the force fields. We obtain better agreement for the polar angle distribution shown in Figure 3 b). The downward facing molecular beam is naturally very narrow with barely any discernible transversal velocity contribution, and purely geometric considerations based on distance between our skimmer and the laser interaction region, the divergence is <1°. The MD simulations account for that by aligning all NO trajectories along the surface normal (black arrow in the right bottom panel in Figure 3 b). The scattered NO molecules – while displaying a wider angular distribution than the molecular beam – still show a surprisingly narrow angular distribution. When fitted to a $\cos^n\theta$ distribution, we obtain a value of 745 for n. A thermal desorption process would yield $n = 1$, indicating that despite the significant loss in kinetic energy, a trapping-desorption mechanism does not seem to play a significant role here. The simulated polar angle distribution follows a $\cos^{49}$ distribution, i.e. a little wider than the experimentally measured distribution, but still very narrow, and much narrower than the angular distributions measured for NO scattered off graphite,[22,23] albeit these were measured at non-zero incidence angles. This demonstrates that both in the experiment and the simulations, a direct scattering mechanism closely along the surface normal is by far the dominant process. We note that the narrow scattering distribution is *not* an artefact of the geometry of our VMI instrument. Since the ionization laser for NO (1+1) REMPI spectroscopy does not need to be focused, we can detect all NO molecules that scatter within a polar angle of 14°, and the majority

of the ionized molecules would follow true VMI conditions due to us using soft extraction conditions with twelve plates.[37] However, it is due to the narrow angular distribution in the experiment, see Figure 4, that we can detect all scattered NO molecules under true VMI conditions.

The MD simulations naturally cannot model reactions between the NO and the graphene, but the results can nevertheless provide information about the trapping-desorption probability. We have directed 4000 trajectories onto graphene and have observed a trapping mechanism for only ~2% of the trajectories. 'Trapping' in this case is for the entire length of each simulation run (4 ps),

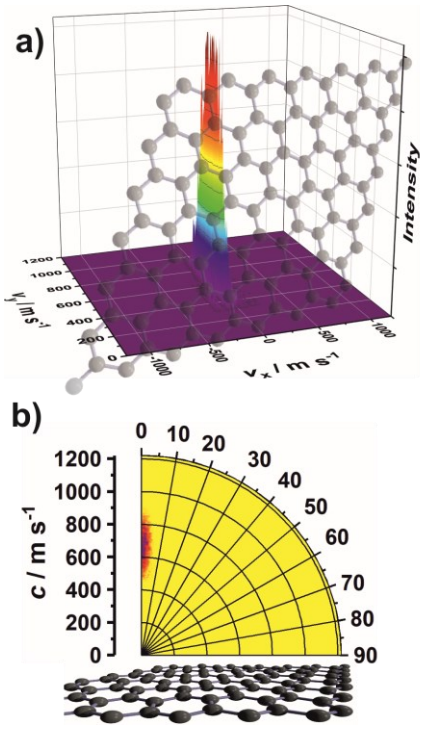

Figure 4: a) Velocity distribution of NO molecules (initial kinetic energy ~0.31 eV) after scattering off graphene resolved along the surface normal (y) and perpendicular to the surface (x, along the propagation direction of the laser). b) Same image, but expressed as speed and polar angle; color range from yellow (=0 intensity) to dark red. Location of graphene schematically indicated in both cases.

but does *not* account for 'double- or multi-bounce' trajectories in which the NO bounces off in a first collision, though does not escape the well and returns to the graphene surface for a further bounce before finally escaping. This 2% trapping probability provides further evidence that trapping-desorption is not a dominant process for normal incidence NO scattering off graphene at kinetic energies of ~0.31 eV.

We can also rule out addition reactions of the NO onto graphene. After exposing the pristine graphene samples to our NO/He molecular beam over a period between two weeks and two months, we performed Raman spectroscopy and X-ray photoelectron spectroscopy (XPS) of the samples before and after exposure. For both techniques, this analysis was done *ex-situ*, i.e. the sample removed from the VMI chamber and transferred to the XPS and Raman instrument in ambient air. Neither did the Raman data indicate the formation of defects (absence of a D peak before and after NO bombardment), nor did the XPS data indicate the addition of N or O species; some oxygen species were present before *and* after NO exposure, but their relative surface coverage did not change.

5. Conclusions

In summary, scattering of ~0.31 eV NO molecules off room-temperature graphene at 0° incidence angle takes away a *significant* amount of kinetic energy from the projectile in a predominantly direct-inelastic process; some of the energy goes into rotation, however, most energy goes into collective motions of the 2D honeycomb lattice of the graphene. This energy loss might be unique to graphene on gold with a fairly large separation of 3.4 Å, with the graphene acting as a 'worn-out trampoline'. Despite this large energy loss, the angular distribution remains *remarkably* narrow, possibly a testament to the flatness of the graphene. However, we expect to learn more about collisional energy transfer processes and the possible

observation of a trapping-desorption mechanism on graphene in future experiments by varying incidence angles and surface temperature.

Acknowledgements:

We thank the Royal Society for funding (IEC\R2\181028), and Prof Nick Lockyer and Dr Mark Dickinson at The University of Manchester for the loan of a frequency-tripling unit. We also thank Christopher Lester for help with the Molecular Dynamics simulations, Dr Alejandro Ferrari for help with the preparation of the graphene samples, and Dilruba Tazmin and Harsimran Singh-Bhaker for assistance during data acquisition. We would also like to thank the reviewers for their insightful comments.

References:

[1] Hynes, J. T. Molecules in Motion: Chemical Reaction and Allied Dynamics in Solution and Elsewhere, *Annu. Rev. Phys. Chem.*, **2015**, *66*, 1.
[2] Murrell, J. N.; Bosanac, S. D. The theory of atomic and molecular collisions, *Chem. Soc. Rev.*, **1992**, *21*, 17.
[3] Valentini, J. J. State-to-state chemical reaction dynamics in polyatomic systems: case studies, *Annu. Rev. Phys. Chem.*, **2001**, *52*, 15.
[4] Kleyn, A. W.; Luntz, A. C.; Auerbach, D. J. Rotational Energy Transfer in Direct Inelastic Surface Scattering: NO on Ag(111), *Phys. Rev. Lett.*, **1981**, *47*, 1169.
[5] Freund, H.-J. The Surface Science of Catalysis and More, Using Ultrathin Oxide Films as Templates: A Perspective, *J. Am. Chem. Soc.*, **2016**, *138*, 8985.
[6] Gordon, M. J.; Qin, X.; Kutana, A.; Giapis, K. P. Gas−Surface Chemical Reactions at High Collision Energies?, *J. Am. Chem. Soc.*, **2009**, *131*, 1927.
[7] Tamtögl, A.; Ruckhofer, A.; Campi, D.; Allison, W.; Ernst, W. E. Atom-surface van der Waals potentials of topological insulators and semimetals from scattering measurements, *Phys. Chem. Chem. Phys.*, **2021**, *23*, 7637.
[8] Cavanagh, R. R.; King, D. S. Rotational- and Spin-State Distributions: NO Thermally Desorbed from Ru(001), *Phys. Rev. Lett.*, **1981**, *47*, 1829.
[9] Oh, J.; Kondo, T.; Arakawa, K.; Saito, Y.; Hayes, W. W.; Manson, J. R.; Nakamura, J. Angular intensity distribution of a molecular oxygen beam scattered from a graphite surface, *J. Phys. Chem. A*, **2011**, *115*, 7089.
[10] Novoselov, K. S.; Fal'ko, V. I.; Colombo, L.; Gellert, P. R.; Schwab, M. G.; Kim, K. A roadmap for graphene, *Nature*, **2012**, *490*, 192.
[11] Geim, A. K. *Science*, Graphene: Status and Prospects, **2009**, *324*, 1530.
[12] AlSalem, H. S.; Holroyd, C.; Danial Iswan, M.; Horn, A. B.; Denecke, M. A.; Koehler, S. P. K.; Characterisation, coverage, and orientation of functionalised graphene using sum-frequency generation spectroscopy, *Phys. Chem. Chem. Phys.*, **2018**, *20*, 8962.

[13] AlSalem, H. S.; Just-Baringo, X.; Larrosa, I.; Monteverde, U.; Jiang, X.; Feng, Y.; Koehler, S. P. K.; Evidence for Site-Specific Reversible Hydrogen Adsorption on Graphene by Sum-Frequency Generation Spectroscopy and Density Functional Theory, *J. Phys. Chem. C*, **2019**, *123*, 25883.
[14] Mehta, N. A.; Murray, V. J.; Xu, C.; Levin, D. A.; Minton, T. K. Nonreactive Scattering of N2 from Layered Graphene Using Molecular Beam Experiments and Molecular Dynamics, *J. Phys. Chem. C*, **2018**, *122*, 9859.
[15] Majumder, M.; Bhandari, H. N.; Pratihar, S.; Hase, W. L. Chemical Dynamics Simulation of Low Energy N_2 Collisions with Graphite, *J. Phys. Chem. C*, **2018**, *122*, 612.
[16] Nieman, R.; Spezia, R.; Jayee, B.; Minton, T. K.; Hase, W. L.; Guo, H. Exploring reactivity and product formation in N(4S) collisions with pristine and defected graphene with direct dynamics simulations, *J. Chem. Phys.*, **2020**, *153*, 184702.
[17] Jayee, B.; Nieman, R.; Minton, T. K.; Hase, W. L.; Guo, H. Direct Dynamics Simulations of Hyperthermal O(^{3}P) Collisions with Pristine, Defected, Oxygenated, and Nitridated Graphene Surfaces, *J. Phys. Chem. C*, **2021**, *125*, 9795.
[18] Santamaría, A. R.; Alducin, M.; Muiño, R. D.; Juaristi, J. I. Ab Initio Molecular Dynamics Study of Alignment-Resolved O_2 Scattering from Highly Oriented Pyrolytic Graphite, *J. Phys. Chem. C*, **2019**, *123*, 31094.
[19] Barker, J. A.; Auerbach, D. J. Gas-surface interactions and dynamics; Thermal energy atomic and molecular beam studies, *Surf. Sci. Rep.*, **1984**, *4*, 1.
[20] Lin, M. C.; Ertl, G. Laser Probing of Molecules Desorbing and Scattering from Solid Surfaces, *Ann. Rev. Phys. Chem.*, **1986**, *37*, 587.
[21] Häger, J.; Fink, M.; Walther, H. Scattering of NO from a graphite surface at cryogenic temperatures, *Surf. Sci.*, **2004**, *550*, 35.
[22] Nyman, G.; Holmlid, L.; Pettersson, J. B. C. Surface scattering of NO from graphite: A statistical description of energy distributions, *J. Chem. Phys.*, **1990**, *93*, 845.
[23] Frenkel, F.; Häger, J.; Krieger, W.; Walther, H.; Ertl, G.; Segner, J.; Vielhaber, W. Rotational state populations and angular distributions on surface scattered molecules: NO on graphite, *Chem. Phys. Lett.*, **1982**, *90*, 225.
[24] Kim, H.; Balgar, T.; Hasselbrink, E. The stretching vibration of hydrogen adsorbed on epitaxial graphene studied by sum-frequency generation spectroscopy, *Chem. Phys. Lett.*, **2011**, *508*, 1.
[25] Nieman, R.; Aquino, A. J. A.; Lischka, H. Exploration of Graphene Defect Reactivity toward a Hydrogen Radical Utilizing a Preactivated Circumcoronene Model, *J. Phys. Chem. A*, **2021**, *125*, 1152.
[26] Jiang, H. Y.; Kammler, M.; Ding, F. Z.; Dorenkamp, Y.; Manby, F. R.; Wodtke, A. M.; Miller, T. F.; Kandratsenka, A.; Bünermann, O. Imaging covalent bond formation by H atom scattering from graphene, *Science*, **2019**, *364*, 379.
[27] Jiang, H.; Tao, X.; Kammler, M.; Ding, F.; Wodtke, A. M.; Kandratsenka, A.; Miller, III, T. F.; Bünermann, O. Small Nuclear Quantum Effects in Scattering of H and D from Graphene, *J. Phys. Chem. Lett.*, **2021**, *12*, 1991.
[28] Chandler, D.; Houston, P. Two-dimensional imaging of state-selected photodissociation products detected by multiphoton ionization, *J. Chem. Phys.*, **1987**, *87*, 1445.
[29] Eppink, A. T. J. B.; Parker, D. H. Velocity map imaging of ions and electrons using electrostatic lenses: Application in photoelectron and photofragment ion imaging of molecular oxygen, *Rev. Sci. Instrum.*, **1997**, *68*, 3477.
[30] Koehler, S. P. K.; Ji, Y.; Auerbach, D. J.; Wodtke, A. M. Three-dimensional velocity map imaging of KBr surface photochemistry, *Phys. Chem. Chem. Phys.*, **2009**, *11*, 7540.
[31] Sporleder, D.; Wilson, D. P.; White, M. G. Final State Distributions of O_2 Photodesorbed from TiO_2(110), *J. Phys. Chem. C*, **2009**, *113*, 13180.
[32] Roscioli, J. R.; Bell, D. J.; Nelson, D. J.; Nesbitt, D. J. State-resolved velocity map imaging of surface-scattered molecular flux, *Phys. Chem. Chem. Phys.*, **2012**, *14*, 4070.
[33] Hadden, D. J.; Messider, T.M.; Leng, J. G.; Greaves, S. J. Velocity map imaging the scattering plane of gas surface collisions, *Rev. Sci. Instrum.*, **2016**, *87*, 106104.
[34] Harding, D. J.; Neugebohren, J.; Hahn, H.; Auerbach, D. J.; Kitsopoulos, T. N.; Wodtke, A. M. Ion and velocity map imaging for surface dynamics and kinetics, *J. Chem. Phys.*, **2017**, *147*, 013939.
[35] Abujarada, S.; AlSalem, H.; Chohan, U. K.; Draper, G. L.; Koehler, S. P. K.; Photodesorption of NO from Au(100) using 3D surface-velocity map imaging, *J. Chem. Phys.*, **2016**, *145*, 184201.
[36] Abujarada, S.; Flathmann, C.; Koehler, S. P. K. Translational and Rotational Energy Distributions of NO Photodesorbed from Au(100), *J. Phys. Chem. C*, **2017**, *121*, 19922.

[37] Abujarada, S.; Walton, A.; Thomas, A.; Chohan, U. K.; Koehler, S. P. K. Adsorption site, orientation and alignment of NO adsorbed on Au(100) using 3D-velocity map imaging, X-ray photoelectron spectroscopy and density functional theory, *Phys. Chem. Chem. Phys.*, **2019**, *21*, 10939.
[38] Reid, M.; Koehler, S. P. K. Validation of velocity map imaging conditions over larger areas*, Rev. Sci. Instrum.*, **2013**, *84*, 044101.
[39] Ji, Y.; Koehler, S. P. K.; Auerbach, D. J.; Wodtke, A. M. Surface three-dimensional velocity map imaging: A new technique for the study of photodesorption dynamics, *J. Vac. Sci. Technol. A*, **2010**, *28*, 807.
[40] Wilkinson, I.; de Miranda, M. P.; Whitaker, B. J. Photodissociation of NO_2 in the (2) $^2B_2$ state: The $O(^1D_2)$ dissociation channel, *J. Chem. Phys.*, **2009**, *131*, 054308.
[41] Todorov, I. T.; Smith, W.; Trachenko, K.; Dove, M. T. DL_POLY_3: new dimensions in molecular dynamics simulations via massive parallelism, *J. Mater. Chem.*, **2006**, *16*, 1911.
[42] Titantah, J. T.; Karttunen, M. Multiphase density functional theory parameterization of the interatomic potential for silver and gold, *Eur. Phys. J. B*, **2013**, *86*, 1.
[43] Kalosakas, G.; Lathiotakis, N. N.; Galiotis, C.; Papagelis, K. In-plane force fields and elastic properties of graphene, *J. Appl. Phys.*, **2013**, *113*, 134307.
[44] Mishra, S.; Meuwly, M. Nitric Oxide Dynamics in Truncated Hemoglobin: Docking Sites, Migration Pathways, and Vibrational Spectroscopy from Molecular Dynamics Simulations, *Biophys. J.*, **2009**, *96*, 2105.
[45] Rappe, A. K.; Casewit, C. J.; Colwell, K. S.; Goddard, W. A.; Skiff, W. M. UFF, a full periodic table force field for molecular mechanics and molecular dynamics simulations, *J. Am. Chem. Soc.*, **1992**, *114*, 10024.
[46] Helgee, E. E.; Isacsson, A. Adsorption of metal atoms at a buckled graphene grain boundary using model potentials, *AIP Adv.*, **2016**, *6*, 015210.
[47] Yin, R.; Zhang, Y.; Jiang, B. Strong Vibrational Relaxation of NO Scattered from Au(111): Importance of the Adiabatic Potential Energy Surface, *J. Phys. Chem. Lett.*, **2019**, *10*, 5969.
[48] Wille, S.; Jiang, H.; Bünermann, O.; Wodtke, A. M.; Behler, J.; Kandratsenka, A. An experimentally validated neural-network potential energy surface for H-atom on free-standing graphene in full dimensionality, *Phys. Chem. Chem. Phys.*, **2020**, *22*, 26113.
[49] Santamaría, A. R.; Ramos, M.; Alducin, M.; Busnengo, H. F.; Muiño, R. D.; Juaristi, J. I. High-Dimensional Atomistic Neural Network Potential to Study the Alignment-Resolved O2 Scattering from Highly Oriented Pyrolytic Graphite, *J. Phys. Chem. A*, **2021**, *125*, 2588.
[50] Rahinov, I.; Cooper, R.; Yuan, C.; Yang, X.; Auerbach, D. J.; Wodtke, A. M. Efficient vibrational and translational excitations of a solid metal surface: State-to-state time-of-flight measurements of HCl (v = 2 , J = 1) scattering from Au(111), *J. Chem. Phys.*, **2008**, *129*, 214708,
[51] Rettner, C. T.; Schweizer, E. K.; Mullins, C. B. Desorption and trapping of argon at a 2H–W(100) surface and a test of the applicability of detailed balance to a nonequilibrium system, *J. Chem. Phys.*, **1989**, *90*, 3800.
[52] Baule, B. *Ann. Phys.*, **1914**, *349*, 145.
[53] Bonfanti, M.; Martinazzo, R. *Int. J. Quantum Chem.*, **2016**, *116*, 1575.
[54] Patel, E.-H.; Williams, M. A.; Koehler, S. P. K. Kinetic energy and angular distributions of He and Ar atoms evaporating from liquid dodecane, *J. Phys. Chem. B*, **2017**, *121*, 233.
[55] Kimman, J.; Rettner, C. T.; Auerbach, D. J.; Barker, J. A.; Tully, J. C. Correlation between Kinetic-Energy Transfer to Rotation and to Phonons in Gas-Surface Collisions of NO with Ag(111), *Phys. Rev. Lett.*, **1986**, *57*, 2053.
[56] Häger, J.; Roth, C.; Fink, M.; Walther, H. Scattering of rotationally excited NO molecules from a graphite surface, *Chem. Phys. Lett.*, **1992**, *189,* 420.
[57] Häger, J.; Shen, Y. R.; Walther, H. State-selective velocity and angular distributions of NO molecules scattered from a graphite surface, *Phys. Rev. A*, **1985**, *31*, 1962.
[58] Golibrzuch, K.; Shirhatti, P. R.; Rahinov, I.; Auerbach, D. J.; Wodtke, A. M.; Bartels, C. Incidence Energy Dependent State-to-State Time-of-Flight Measurements of NO(v = 3) Collisions with Au(111): the Fate of Incidence Vibrational and Translational Energy, *Phys. Chem. Chem. Phys.*, **2014**, *16*, 7602.
[59] Cooper, R.; Bartels, C.; Kandratsenka, A.; Rahinov, I.; Shenvi, N.; Golibrzuch, K.; Li, Z.; Auerbach, D. J.; Tully, J. C.; Wodtke, A. M. Multiquantum Vibrational Excitation of NO Scattered from Au(111): Quantitative Comparison of Benchmark Data to Ab Initio Theories of Nonadiabatic Molecule–Surface Interactions, *Angew. Chem.*, **2012**, *51*, 4954.